JGR Oceans

RESEARCH ARTICLE
10.1029/2019JC015858

Increased Mixing and Turbulence in the Wake of Offshore Wind Farm Foundations

L. K. P. Schultze[1], L. M. Merckelbach[1], J. Horstmann[1], S. Raasch[2], and J. R. Carpenter[1]

[1]Helmholtz-Zentrum Geesthacht, Institute of Coastal Research, Geesthacht, Germany, [2]Institute of Meteorology and Climatology, Leibniz Universität Hannover, Hannover, Germany

Key Points:
- Enhanced mixing and disturbed stratification in the wake of monopiles is traceable in field and turbulence-resolving numerical experiments
- Elevated turbulent dissipation and mixing are found in a narrow region downstream of monopiles, with a bulk mixing efficiency of 8–14%
- The enhanced mixing generated by the offshore wind farm structures could contribute to significant changes in stratification in shelf seas

Correspondence to:
L. K. P. Schultze,
larissa.schultze@hzg.de

Citation:
Schultze, L. K. P., Merckelbach, L. M., Horstmann, J., Raasch, S., & Carpenter, J. R. (2020). Increased mixing and turbulence in the wake of offshore wind farm foundations. *Journal of Geophysical Research: Oceans*, *125*, e2019JC015858. https://doi.org/10.1029/2019JC015858

Received 8 NOV 2019
Accepted 19 JUN 2020
Accepted article online 25 JUN 2020

The copyright line for this article was changed on 26 MAR 2021 after original online publication.

Abstract The addition of offshore wind farms (OWFs) to stratified regions of shelf seas poses an anthropogenic source of turbulence, in which the foundation structures remove power from the oceanic flow that is fed into turbulent mixing in the wake downstream. The loss of stratification within the wake of a single OWF structure is observed for the first time by means of field observations, which enable a qualitative characterization of the disturbed flow downstream. These results are complemented with high-resolution large eddy simulations of four different stratification strengths that allow for a quantification of turbulence and mixing quantities in the wake of a foundation structure. The turbulent wake of a structure is narrow and highly energetic within the first 100 m, with the dissipation of turbulent kinetic energy well above background levels downstream of the structure. A single monopile is responsible for 7–10% additional mixing to that of the bottom mixed layer, whereby ~10% of the turbulent kinetic energy generated by the structure is used in mixing. Although the effect of a single turbine on stratification is relatively low, large-scale OWFs could significantly affect the vertical structure of a weakly stratified water column. Further, rough estimates show that the rate of formation of stratification in the study area is of the same order of magnitude as the additional mixing promoted by the structures, thus OWFs could modify the stratification regime and water column dynamics on a seasonal scale, depending on local conditions and farm geometries.

Plain Language Summary Advances in the renewable energy sector have enabled the construction and operation of wind farms in bodies of water deep enough to present vertical temperature differences across the water column or thermal stratification. In coastal regions dominated by tidal motion, the presence of offshore wind farm (OWF) structures brings about additional turbulence and mixing of stratification. The present study combines field measurements and numerical simulations to characterize the wake of single OWF structures and quantify the amount of turbulence and mixing generated by them. Our results suggest that the effect of OWF structures is small compared to other naturally occurring mixing mechanisms, however can be comparable to the rate of stratification buildup. Stratification in certain regions of shelf seas could be impacted by OWFs if these are built over a large area.

1. Introduction

The reduction of greenhouse gas emissions through the advancement and promotion of renewable energy technologies is one of the strategies that have been adopted for the mitigation of anthropogenic climate change. The created legal frameworks, together with a series of governmental incentives, have facilitated the growth and development of offshore wind technology worldwide. Within the European Union (EU), a total of 15.8 GW have been installed and connected to the grid until December 2017, and the installation of an additional 10 GW has been planned (Wind Europe et al., 2018). Among the relevant sea basins for the construction of offshore wind farms (OWFs), the North Sea leads as the most important basin, with 71% of the total offshore wind capacity within the EU (Wind Europe et al., 2018).

Advances in the offshore wind sector have allowed the construction of OWFs in deeper waters further away from the coast, where stronger winds are found. While in 2013 the mean depth of OWFs was 16 m, in 2017 the mean depth reached 27.5 m (Corbetta et al., 2014; Wind Europe et al., 2018), and therefore, they increasingly affect areas that undergo thermal stratification. This study focuses on the impact of offshore wind farm

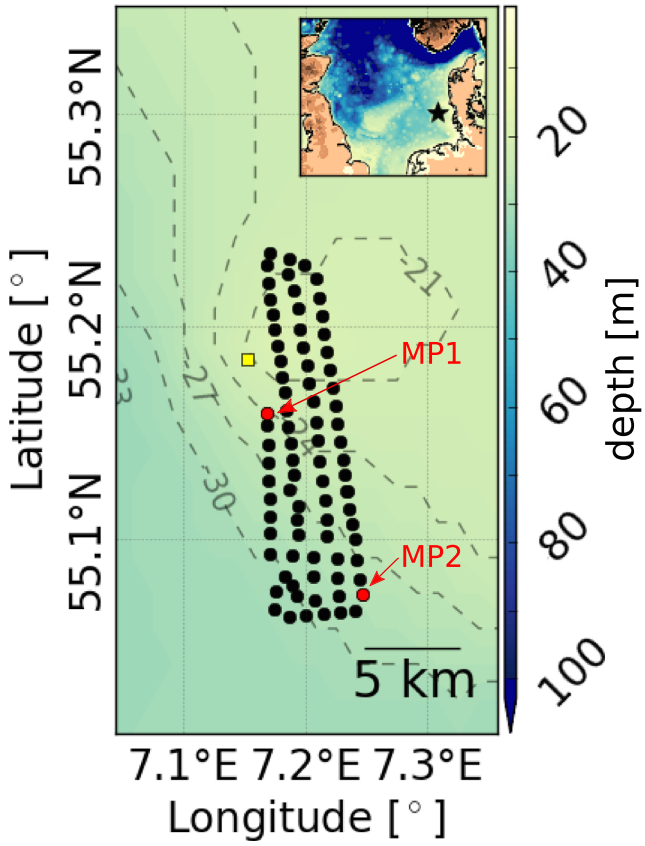

Figure 1. Plan of the offshore wind farm DanTysk with single monopiles shown as black dots. The red dots mark the monopiles surveyed with the towed chain, with the monopile MP1 situated on the left side of the depicted farm, and the monopile MP2 on the bottom right. The map on the top right corner of the figure shows the North Sea and indicates the position of DanTysk through the black star. The colorbar depicts depth across the whole North Sea and the gray dashed contour lines detail depth in the study area. The position of the platform FINO3 is shown through the yellow square.

structures on turbulence and its mixing of stratification. The German Bight of the southern North Sea is used as the study region due to its relevance in the offshore wind energy sector.

1.1. Seasonal Stratification and Mixing by OWFs

The German Bight is situated in a relatively shallow area of the North Sea with typical water depths between 20 and 50 m (Figure 1). In this region, thermal stratification often occurs during the summer months, whereas saline stratification is concentrated close to coastal areas (Huthnance, 1991). Seasonal stratification in shelf seas is known to reduce vertical fluxes, controlling nutrient transport to the upper layer and therefore primary production (Simpson & Sharples, 2012). This has an influence on the storage and export of carbon dioxide through the shelf sea pump (Thomas et al., 2004). Quantifying stratification and how it is affected by different sources of mixing in shelf seas is therefore of major global and societal importance.

Shelf seas are often strongly influenced by tidal motion, which, with the presence of OWF foundation structures in the water column, will repeatedly drive currents through the structures and potentially lead to enhanced turbulent mixing within their wake. This “egg beater” mixing mechanism is in addition to the naturally occurring processes acting upon the stratification. However, it remains largely unknown if OWF mixing is significant in altering stratification in shelf seas. There are a few analytical and numerical studies characterizing the hydrodynamic impacts of OWFs available in the literature (e.g., Broström, 2008; Grashorn & Stanev, 2016; Ludewig, 2015; Paskyabi, 2015; Paskyabi & Fer, 2012; Roulund et al., 2005). However, most studies focus on the wind wake and the resulting generation of upwelling/downwelling cells in the water column, or the wake generated in a neutrally stratified water column.

Rennau et al. (2012) have studied the influence of offshore wind farm structures on dense bottom currents in the Baltic Sea using the Reynolds-averaged Navier-Stokes (RANS) equations with the k-ε turbulence closure scheme. The grid used was circular and highly resolved within three cylinder diameters (d) and transformed to a rectangular shape within the next 3d. The simulations with realistic setups have found that OWF-induced mixing was expected to be relatively low, decreasing the salinity at the bottom by 0.1–0.3 PSU, which is below natural variability (Rennau et al., 2012). Cazenave et al. (2016) used an unstructured grid model to study single turbine foundations in the context of the shelf sea circulation, focusing mostly on the Irish Sea. The simulations included both well-mixed and stratified periods, and the grid resolution varied between 2.5 and 20 m depending on the run and on the distance from the turbine foundation. The RANS equations are used to describe the turbulent flow, and turbulence closure is again obtained through a k-ε scheme. With the modeled setup, vertical mixing was enhanced by the foundations up to a 200 m distance, and an OWF was found to possibly affect the stratification by 5–15% over an area nearly 80,000 times the total footprint of its monopiles, which in this study corresponded to 3,180 m^2 (Cazenave et al., 2016).

While Rennau et al. (2012) and Cazenave et al. (2016) provided a first attempt to characterize the OWF-induced mixing of stratification, shortcomings in RANS models are present regarding the parameterization of turbulence and its suitability for detailed turbulence studies involving density-stratified conditions and obstacles. These limitations can be overcome through large eddy simulations (LES), in which the large, energy-containing, turbulent scales are explicitly resolved, with the smaller scales parameterized. The need for LES in tackling this problem arises due to the injection of turbulent kinetic energy at the scale of the OWF foundation structure, with the largest eddies being on scale of the diameter of the foundation structure. To properly capture variations in the flow generated by the structure, a grid resolution sufficiently smaller than the diameter of a monopile is needed, and these overlap with the largest turbulent eddies.

Carpenter et al. (2016) conducted an idealized study to assess the large-scale impact of OWFs on stratification in tidal shelf seas. According to their study, a significant decrease in stratification in the North Sea could take place if a considerable portion of the shelf would be filled with OWFs. A central unknown in their analysis was the bulk mixing efficiency of the OWF structures, that is, the fraction of the total turbulent kinetic energy production that is delivered to mixing the stratification. The estimation of this quantity is a central goal of the present study that will allow for a better assessment of the possible impact that OWF structure mixing has on shelf sea stratification.

Using the averaged estimates of the power extracted from the flow by OWF foundation structures presented in Carpenter et al. (2016), Schultze et al. (2017) calculated the average dissipation rate of turbulent kinetic energy that can be expected from the OWF structures, $\langle \varepsilon_{OWF} \rangle$, and compared it with field observations of turbulence. The $\langle \varepsilon_{OWF} \rangle$ was estimated to be comparable to turbulence levels found in the thermocline. The power production by OWFs, and therefore also the dissipation rate of turbulent kinetic energy, were estimated assuming that a large section of the shelf would be covered with OWFs and should be interpreted as average values over the entire region. In reality, the intensity of production and dissipation of turbulent kinetic energy by single turbines are not expected to be equally distributed over a large area, but to be mostly concentrated in the wake of each structure. Furthermore, the increase in vertical mixing on the wake of the OWF foundations could be significant, with possible changes in vertical stratification, nutrient, and sediment concentrations that could affect the ecosystem (Carpenter et al., 2016; Schultze et al., 2017).

Toward this aim, Floeter et al. (2017) have assessed biophysical parameters in two OWFs in the German Bight of the North Sea while the water column was stratified. Empirical evidence of enhanced vertical mixing was found, predicting higher nutrient fluxes to the surface layer. Field observations that characterize the physical impact of OWFs are however rare, and it is especially challenging to discern the signal of the OWF from natural variability (Floeter et al., 2017).

Given the increased interest in OWF technology and their potential to alter turbulence and mixing levels, we conduct a small-scale study of the near-field stratified wake to assess the importance of this additional turbulence source. The present study uses field observations and a large eddy simulation model to assess turbulence and mixing induced by an OWF foundation structure. Although the amount of mixing generated by OWFs is expected to depend on the type of foundation structure considered, the monopiles, which are vertical circular cylinders, are the most relevant within the EU, with a share of 87%. Therefore, this study focuses on the possible impact of a monopile on the mixing of a stratified water column.

The present study is organized as follows: Section 2.1 gives an overview of the field experiments and equipment used, with findings presented in section 2.2. To compare the field observations with numerical modeling, and to gain more information about the stratified wake, LES are used. The large eddy simulation model and the setup of the simulations are briefly described in section 3. The LES were designed to resemble the conditions found in the field experiments, of which results are presented in section 3.2. A general discussion and the conclusions of this study are presented in sections 4–6.

2. Field Observations

2.1. Overview of Field Experiments and Equipment

Field measurements in the OWF DanTysk in the German Bight of the southern North Sea were conducted in two different years, 2015 and 2017, during the summer stratified period. The OWF DanTysk is centered at 55.14°N and 7.20°E, and was primarily chosen because it is composed of monopiles, the turbine foundation of interest, which have 6 m diameter. A further advantage of DanTysk is the occurrence of vertical density stratification, despite the fact that the water depth within the farm is relatively low, ranging from 20–30 m (Figure 1).

Before the surveys were conducted, tidal times, direction, and height were analyzed and a single monopile was selected each day for the wake analysis. In 2015, the survey took place on 25 May between approximately 12:10 and 12:40 p.m. UTC, and the chosen monopile, hereafter MP1, was situated at 55.16°N and 7.17°E (Figure 1). Conversely, in 2017, the monopile at 55.07°N and 7.25°E was selected (MP2), and the survey was conducted on 19 July between 09:20 and 10:40 a.m. UTC (Figure 1).

The wake of the monopile was surveyed using a chain of conductivity, temperature, and depth (CTD) sensors measuring with a frequency of 10 Hz, which was towed from a Zodiac in 2015. Hereafter, the chain of CTD sensors is referred to as the towed chain. In 2015, the towed chain was composed of six sensors that were fixed 1–2 m apart from each other and measured from 1.5 to 8 m depth. In 2017, the wave heights reached over 2.5 m, such that deploying the Zodiac became unfeasible. Therefore, in 2017, the towed chain was attached to the RV Ludwig Prandtl, which had its rear propeller switched off as it surveyed the monopile to avoid the contamination of the measurements. During this experiment, eight sensors placed 1.5 m apart from each other were attached to the towed chain between 3.5 and 14 m depth. On both field experiments, the CTD sensors used were manufactured by Sea & Sun Technology GmbH.

Additionally, we have used the temperature data measured by sensors available at the fixed platform FINO3, which is located in the vicinity of DanTysk (Figure 1). At FINO3, the water temperature is recorded at three different depths (6, 12, and 18 m). The temperature data are available at the FINO database (http://fino.bsh.de/), which is maintained by the German Maritime and Hydrographic Agency (Bundesamt für Seeschifffahrt und Hydrographie, BSH).

2.2. Observations of the Monopile Wake

Weak stratification. The monopile surveyed in 2015 was situated in a shallow area of ∼24 m depth that was weakly stratified with 0.5°C difference between the sea surface and the bottom mixed layer, which reached to ∼10 m depth. At the time of the measurements, the monopile was situated on the upstream side of the OWF, with the current coming from the Northwest with a mean current direction and speed of 127° and 0.3 m s^{-1}, respectively. The wind speeds were between 5 and 7 m s^{-1} at 10 m height.

Figure 2a shows the temperature measured by the different sensors fixed to the towed chain in time. The vertical separation of the lines shows the background temperature structure, where the temperature decreased with depth. Overlapping areas in which all sensors measured similar temperature are highlighted in blue and indicate a disruption of the background temperature structure. The same areas are identified if salinity or density estimates are considered (not shown). Further, the disturbed regions follow a coherent pattern that can be identified as the wake region downstream of the monopile. This can be seen in Figure 2b along with their respective vertical temperature profiles averaged over the wake region at different distances from the monopile (Figure 2c), which are marked in red, orange, yellow, green, light blue, and navy blue. For comparison, the background temperature structure of the water column during the measurement period was taken as the average temperature at each measured depth outside the wake of the structure. Similar to the wake regions, the averaged vertical profile of background temperature in the studied period of 2015 is shown in Figure 2c along with its standard deviation.

The monopiles, and OWF structures in general, are expected to contribute to the mixing of the water column by extracting energy from the flow and feeding it into the small-scale turbulence responsible for mixing. In our measurements in 2015, the disruption of background stratification by the wake is observed within a narrow region of up to 70 m width that reaches at least 300 m downstream of the monopile. Although no measurements were taken further downstream of the wake, the vertical profile obtained at ∼500 m exhibits a stronger temperature gradient than the previous profiles between 200 and 350 m. This could be an indication that the turbulence produced by the monopile has decayed sufficiently for restratification to occur. This is supported through the calculation of the background potential energy anomaly $\varphi = g\int(\rho' - \rho'_{mix})z\mathrm{d}z$, where z is the depth, ρ' the sorted density, and $\rho'_{mix} = 1/H\int\rho'(z)\mathrm{d}z$ is the density of the mixed water column, with H the water depth in meters. The quantity φ has been introduced by Simpson and Bowers (1981), and it calculates the amount of energy necessary to mix a stratified water column. Further, the higher the φ, the stronger the stable stratification and φ=0 if the water column is fully mixed. To calculate φ based on the towed chain measurements, it was assumed that the density outside the measured depth range remained unchanged from the last data point. This assumption is supported by the data collected at the platform FINO3 (Figure 2a). Within the wake of the monopile, φ decreased by up to 35% at 250 m, after which the strength of stratification increased again (not shown).

Strong stratification. Similar to 2015, the monopile selected for analysis in 2017 was situated on the upstream edge of the OWF in a 27–30 m depth region. The temperature reached 17.2°C near the sea surface and decreased to 15.1°C until 18 m depth. Wind speeds were about 7 m s^{-1} and the ocean current direction and

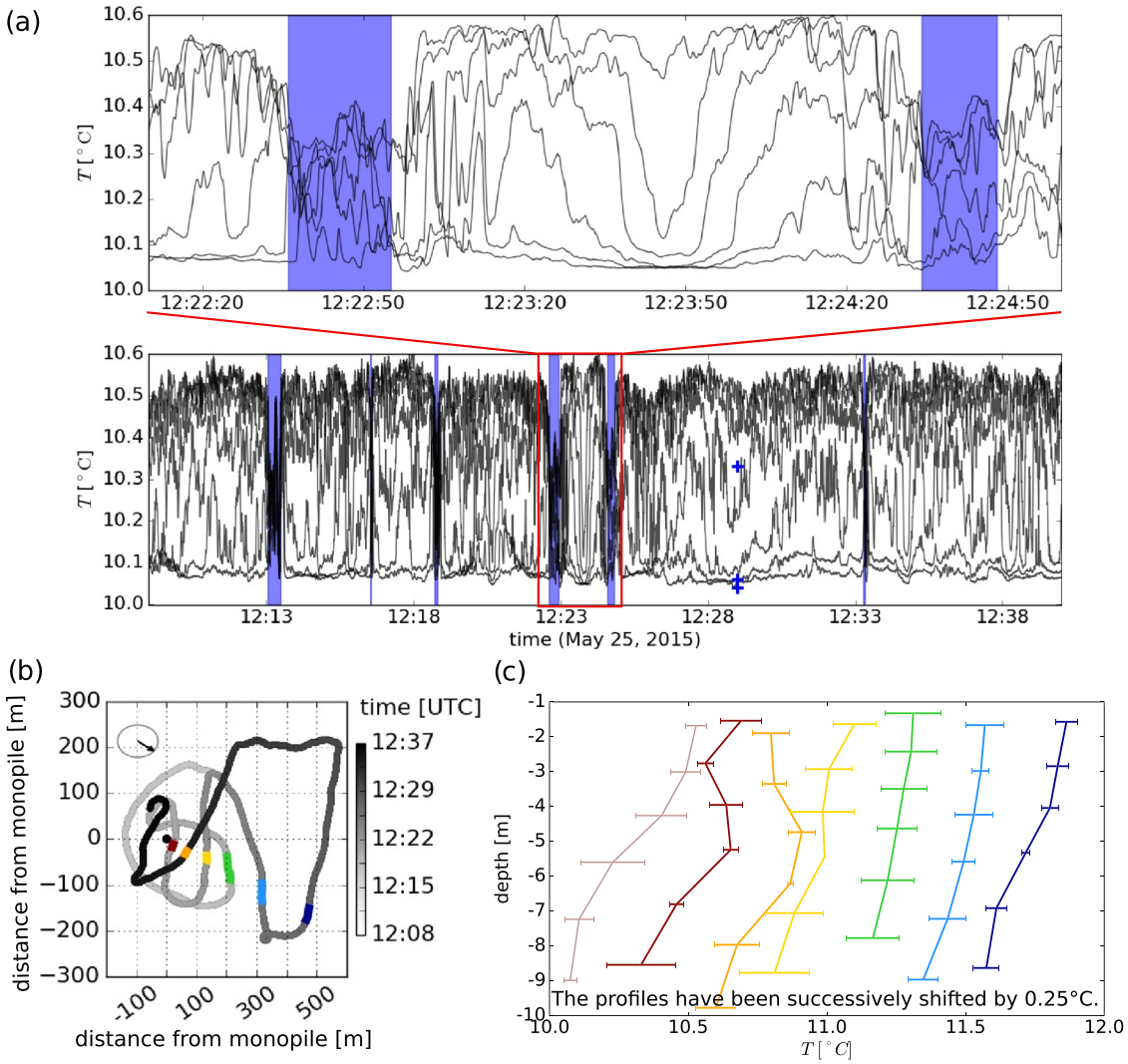

Figure 2. (a) Time series of the towed chain temperature measurements in 2015 in weak stratification. The complete time series is shown in the bottom panel, whereas the upper panel depicts a zoomed section for better visualization of the effect of the monopile on the vertical structure of the water column. Each black line represents one CTD sensor. Areas in which the temperature measured by the sensors overlap are marked blue. The blue crosses in the second panel show the temperature measured at the research platform FINO3 at water depths of 6, 12, and 18 m. (b) Measurement path of the towed chain. The position of the blue sections marked in (a) are shown by the red, orange, yellow, green, blue, and dark blue lines, following their line of occurrence. The black arrow on the top left corner depicts the mean ocean current direction. (c) The temperature structure of the water column within the wake of the monopile was considerably disturbed within a narrow area. The gray line represents the vertical temperature structure of the water column averaged outside the wake region ("background conditions"), with 1 standard deviation shown by the error bars. The background conditions are taken to be the entire time series of data collected, except for the sections highlighted blue in (a). Vertical profiles of temperature averaged over the sections marked in (b) within the wake of the monopile are shown for the respective color-coded sections. The profiles in (c) have been successively offset by 0.25°C from each other for better visualization.

speed were 305° and 0.3 m s^{-1}, respectively. Despite having tracked the region of the monopile wake, no clear signal from the monopile could be identified that stood out from the naturally occurring variability (not shown). Opposed to 2015, where the focus was laid up to about 500 m from the monopile, the analyzed region in 2017 extended over 1,000 m downstream from the monopile with cross sections that were ~200 m apart from each other. No clear influence of the monopile was observed in the cross section at 400 m or at 200 m downstream, which is the closest that the measurements came to the monopile on that experiment (not shown).

The observations with the towed chain have provided evidence that, depending on the strength of stratification, single monopiles can significantly alter the vertical structure of the water column within its wake. Further, the wake of the obstacle was found to reach a width up to ten times its own diameter. Under

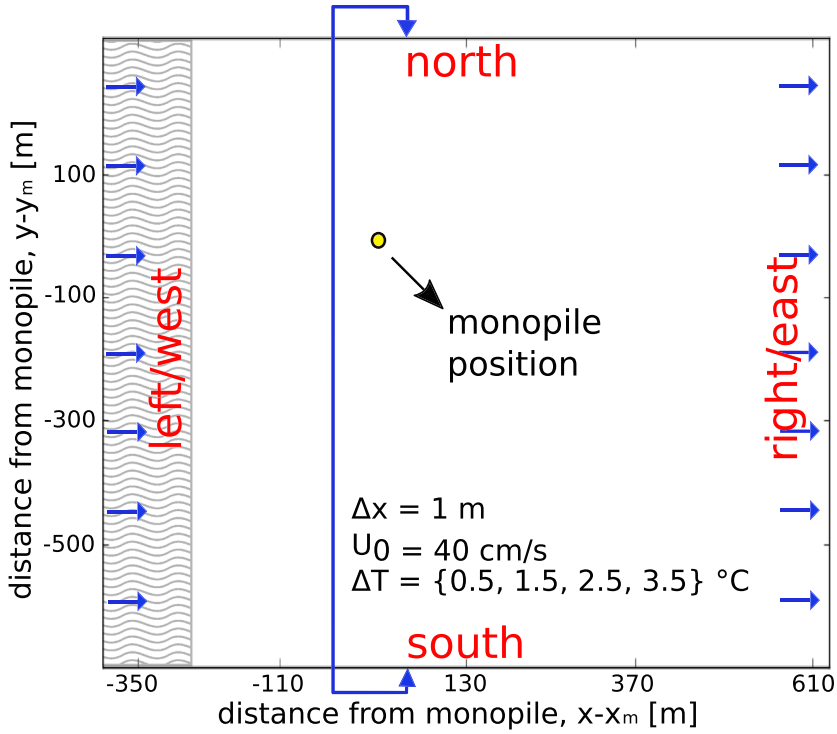

Figure 3. Sketch of the simulation setup. The monopile, located at x_m,y_m, is shown in yellow. The axes have been centered at the monopile location. The simulations were run using cyclic boundary conditions on the north and south boundaries, which is indicated by the blue arrow. West and east boundaries were inflow and outflow conditions. The hatched pattern marks the turbulence recycling domain.

weak stratification, the disturbance of the vertical structure of the water column by the wake reached at least 450 m downstream, after which restratification of the wake region began. To enable the quantification of mixing and dissipation of turbulent kinetic energy by single OWF structures, high resolution numerical modeling was performed replicating conditions found in the field measurements. Therefore, the next section describes our approach to analyze the flow downstream from a monopile using LES. These also provide context to better interpret the field observations.

3. Large Eddy Simulations

Studying the wake of a structure in the field is challenging due to difficulties in isolating the natural variability of the flow from the true signal of the structure. To complement the observational evidence obtained through the towed chain measurements, we use LES and assess the wake of a monopile under different levels of stratification with the goal of quantifying turbulence and mixing by the structures under different stratification scenarios. LES resolve the large, energy-containing eddies and filter the small eddies, which are parameterized by means of a subgrid-scale model. This allows the simulation of flows with high Reynolds numbers at grid resolutions on the order of 1 m, and therefore resolves the most important energetic scales of turbulence, which is not possible when using RANS models.

The LES model used is the Parallelized Large-Eddy Simulation Model for atmospheric and oceanic flows (PALM, version 4.0, revision 2504), which has been developed at the Institute of Meteorology and Climatology of the Leibniz University of Hannover (Raasch & Schröter, 2001). PALM is in continuous development, and its most recent thorough description can be found in Maronga et al. (2019).

PALM solves the nonhydrostatic, incompressible Navier-Stokes equations after the Boussinesq approximation. The parameterization of the subgrid scales is performed after (Deardorff, 1980; Moeng & Wyngaard, 1988; Saiki et al., 2000) and considers that the energy transported by small eddies is proportional to the respective gradients of the mean quantities. PALM uses a Cartesian Arakawa staggered C-grid (Arakawa

Table 1
Summary of the Parameters Used in the Simulations to Investigate the Wake of the Monopile, With d the Monopile Diameter, L_x and L_y the Domain Length Along x and y, s the Salinity, T the Temperature, ν the Kinematic Viscosity of Sea Water, and U_0 the Characteristic Flow Velocity

Parameter	Unit	
Domain size, precursor run	[m×m×m]	128 × 512 × 32
Domain size, main run	[m×m×m]	1,024 × 1,024 × 32
Δx_i	[m]	1
d	[m]	7
L_x/d	[-]	146
L_y/d	[-]	146
U_0	[ms^{-1}]	0.4
$Re=U_0d/\nu$	[-]	2.8×10^6
ΔT	[°C]	0.5, 1.5, 2.5, 3.5
s	[PSU]	33

& Lamb, 1977; Harlow & Welch, 1965) with equidistant spacing between the grid cells. The representation of the monopile, a circular cylinder, is therefore approximated in the simulations described below, whereby the resemblance to a real cylinder increases with the grid resolution. The following subsection describes the setup used in the simulations.

3.1. Simulation Setup

The domain size of all simulations used in scientific analysis was 1,024 m × 1,024 m × 32 m, with the grid size Δx_i=1 m in all directions (Figure 3 and Table 1). The grid size was chosen after a grid sensitivity analysis considering Δx_i=2,1,0.5 m, in which similar results referring to changes in stratification and drag coefficient were obtained for the 1 and 0.5 m grids (not shown). To resemble field conditions and realistic spacing between structure foundations, the monopile was positioned at 400 m from the west boundary and at 750 m from the south boundary. At the sea surface, Neumann boundary conditions were used for all velocity components and scalar variables and the Dirichlet (no slip) boundary condition was applied at the sea bed. Further, to be able to isolate the turbulence generated by the monopile from turbulence generated at the sea bed, separate identical simulations tackling solely the impact of bottom boundary layer turbulence (i.e., without the monopile) on stratification were performed.

The south and north boundaries of the domain were assigned periodic conditions and, to investigate the impact of a single monopile on stratification, nonperiodic boundary conditions were applied along the main flow direction (left and right boundaries) for all velocity components and scalar variables (Figure 3). When using nonperiodic boundary conditions, a turbulent inflow has to be defined to trigger bottom boundary layer turbulence generated by friction at the sea bed throughout the entire domain, such that the effect of the obstacle can be separated from other turbulence sources. A turbulent inflow is implemented in PALM through the "turbulence recycling method," in which a precursor simulation with periodic lateral boundary conditions is run until turbulence has developed and the setup has reached a quasi-steady state (Kataoka & Mizuno, 2002; Lund et al., 1998; Maronga et al., 2015). Once the precursor run has reached a quasi-steady state, its output is used to stir the main run. In the present simulations, where the domain size of the main run is greater than that of the precursor run, the output data of the latter is used to fill up the larger domain through cyclic repetition (Maronga et al., 2015). Further, at the inflow boundary of the main run, the turbulence recycling method uses the mean vertical profiles of all velocity components and scalar variables, calculated in the precursor run, and sets Dirichlet boundary conditions. At the outflow, radiation boundary conditions were applied to the velocity components and Neumann boundary conditions for scalars.

The domain size in the precursor simulations was 128 m × 512 m × 32 m, and the same grid size as in the main run was used, Δx_i=1 m (Table 1). A vertically homogeneous current velocity of 0.4 m s^{-1} was attained by imposing a large-scale pressure gradient, which corresponds to typical values found in the study region. Random disturbances up to 10^{-4} m s^{-1} were imposed within the bottom 5 m of the domain to trigger bottom boundary layer turbulence induced by friction. No obstacle was added to the precursor run. Planetary rotation was included in the precursor and main simulations for 54°N latitude to resemble conditions found in the German Bight of the North Sea. No additional heat, wind forcing, or pressure gradient is applied to stir the simulations.

Four different scenarios of vertical stratification were analyzed in this study, all of which have been defined in the precursor runs by a temperature gradient, whereas salinity was kept constant at 33 PSU. The implementation of the stratification in all cases was given by a linear gradient of temperature, which was motivated by field measurements, that is, (i) 1.5°C/10 m; (ii) 2 °C/10 m; (iii) 3 °C/10 m, and (iv) 4 °C/10 m, starting from the top of the domain until 10 m depth. The precursor simulation of each of the four cases was run until the quasi-steady state was reached, at which point some mixing had inevitably already taken place. Therefore, the initial temperature profiles for the respective main runs differ from the initial conditions of the precursor runs and are shown in Figure 4.

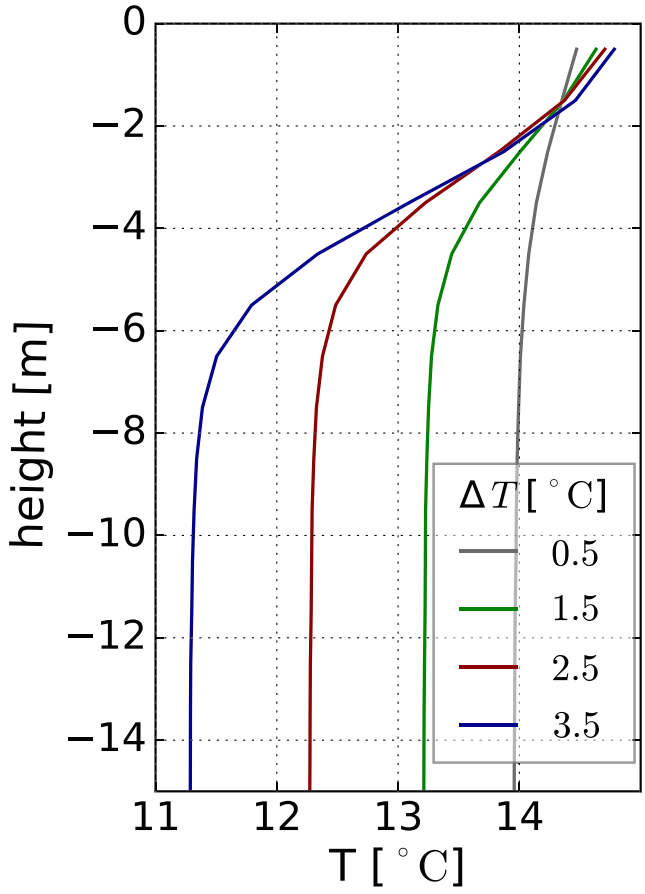

Figure 4. Initial vertical profiles of temperature for the main simulations of the four stratification cases considered, whereby ΔT represents the total change in temperature across the water column for each of the studied cases. No further differences in the profiles were detected below −15 m height.

All main runs analyzed were carried out for ~10 hr simulated time. The quasi-steady state of the simulations was reached at ~2 hr and the remaining 8 hr were used in the calculation of mixing quantities, which are described in the following sections.

3.2. Stratification Anomalies Generated by Wake Turbulence

The weakest (i) to strongest (iv) stratification cases are shown in Figure 5, which depicts the wake of the monopiles close to the sea surface at 0.5 m depth in the context of temperature anomaly compared to the overall vertical temperature difference $\tilde{T}/\Delta T$. Moreover, the temperature anomaly $\tilde{T} = T(x, y) - T(0, y)$ shows how the temperature along the horizontal axes (x and y) at the near-surface depth z=0.5 m changes compared to the inflow temperature $T(0,y)$, at x=0.

The panels in Figure 5 have been centered with respect to the position of the monopile, which can be clearly identified along with its wake generated downstream. In all analyzed cases, the wake of the monopiles can be identified at the surface by a decrease in temperature. The analyzed wakes were 50–100 m (or 7–14d) wide and the disturbances in the flow field and temperature were observed until the end of the domain at 600 m past the monopile.

However, the relative magnitude of the temperature anomalies observed at sea surface compared to the total vertical temperature change decreases with increasing stratification, and forcing toward restratification in the wake region is enhanced (Figure 5). The temperature anomaly generated through monopile-induced mixing largely exceeds 50% (i.e., $\tilde{T}/\Delta T > 0.5$) of the overall vertical temperature difference within the wake in the weakest stratified case (i, Figure 5a). The effect of the monopile mixing compared to the overall temperature gradient is however increasingly masked as stratification increases. In the strongest stratified case (iv), the temperature anomaly promoted by the monopile stays mostly well below 40% that of the total vertical temperature gradient, with a considerably narrower width and length than under weaker stratification (cf. Figures 5a–5d).

Moreover, the greater the temperature gradient, the stronger the forcing toward the stabilization of the wake, which limits the range of influence of the wake downstream. Upstream of the monopile, the water column is being stirred by bottom boundary layer turbulence and the temperature gradient reaches from the sea surface up to 8–10 m depth. As the flow passes by the structure, the water column is further disturbed and vertical motion is enhanced in a narrow region of the domain. These qualitative observations are further analyzed in the next subsections, in which the change in stratification and mixing caused by single monopile structures, as well as the dissipation of turbulent kinetic energy, are quantified.

3.3. Turbulent Mixing in Wakes

As introduced in section 2.2, the amount of energy required to mix the water column can be obtained through the background potential energy anomaly (φ), which quantifies the minimum amount of potential energy in a water column relative to the completely mixed state. Comparably to section 2.2, for the 3-D simulations, φ was calculated for each yz slice corresponding to every grid point in the x direction as

$$\varphi(x) = \frac{g}{L_z}\int [\rho_{mix}(x) - \rho(x, z^*)]z^* \mathrm{d}z^*, \quad \text{with } \rho_{mix}(x) = \frac{1}{L_z}\int \rho(x, z^*)\mathrm{d}z^*. \tag{1}$$

In Equation 1, the model domain is subdivided into volume slices along the x direction, each with dimensions $\Delta x \times L_y \times L_z$. The density of every grid point in a slice is then reordered and sorted into a vector $\rho(x, z^*)$, where z^* is the depth vector with $N_y \times N_z$ equally spaced elements that ranges from 0 to L_z, where L_z

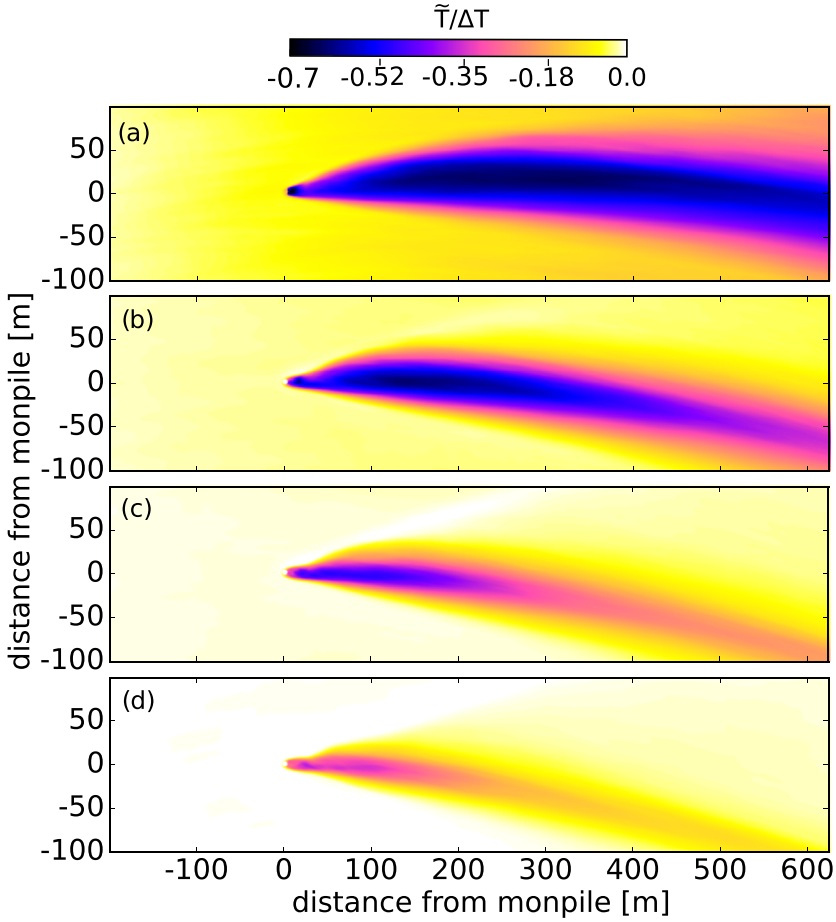

Figure 5. Horizontal cross section at 0.5 m depth of the temperature anomaly relative to the total vertical temperature gradient ($\tilde{T}/\Delta T$) averaged over 5,000 s for all analyzed stratification scenarios, namely: (a) $\Delta T \approx 0.5$°C, (b) $\Delta T \approx 1.5$°C, (c) $\Delta T \approx 2.5$°C, and (d) $\Delta T \approx 3.5$°C. The horizontal axes have been centered to the monopile location and extend from 200 to 1,024 m along the south boundary and 650 to 850 m along the west boundary.

is the total depth of the water column (Burchard & Hofmeister, 2008; Winters et al., 1995). The profile $\rho(x,z^*)$ represents the stratification that would result from an adiabatic rearrangement of the stratification to the state of minimum potential energy. The adiabatically sorted vector $\rho(x,z^*)$ enables the calculation of the minimum amount of potential energy in the slice, which is then used to estimate the amount of energy needed to reach the mixed state $\rho_{mix}(x)$. Thus, through φ, the change in stratification along the domain in the direction of the flow is quantified for each of the simulations.

Figure 6a depicts the loss of stratification attributed to mixing by bottom boundary layer turbulence only (semitransparent dashed lines) and with the addition of the monopile (solid lines). This is done by showing how the background potential energy changes along x, that is, the flow direction, compared to its initial state φ_0. The change in background potential energy in the simulations without the monopile is explained by bottom boundary layer turbulence. In the simulations with the monopile, vertical mixing before the monopile is due to bottom boundary layer turbulence and to a much smaller extent due to an upstream effect of the structure itself, which is intensified at the monopile location and downstream, as shown in Figure 6a by the enhanced drop in φ after the monopile.

The rate of decrease in background potential energy along the domain is equivalent to the mixing rate, that is, $m = \bar{U}(x)\mathrm{d}\varphi/\mathrm{d}x$, with $\bar{U}(x)$ the mean velocity of the respective x slice. Note that when m is averaged over times long enough that no net changes in the available potential energy occur, the mean m is equivalent to the mean buoyancy flux (see Winters et al., 1995). The total mixing within the domain is obtained by

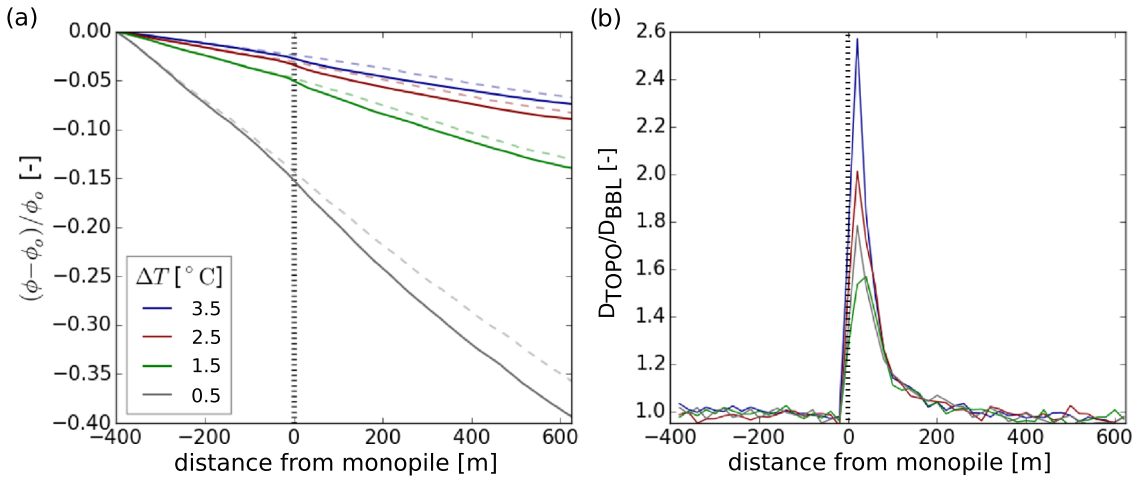

Figure 6. Change in background potential energy (a) and in the ratio of total dissipation of turbulent kinetic energy in the simulations with the monopile by the ones without it (D_{TOPO}/D_{BBL}) (b) for cases (i)–(iv) along the domain length (x axis), which has been centered with respect to the position of the monopile. In (a), solid lines depict results of simulations with the obstacle, whereas dashed lines show the change in background potential energy for the simulations without the structure. The color code in (b) is the same as in (a); however, each line stand for the ratio D_{TOPO}/D_{BBL} of a given case, with D_{TOPO} and D_{BBL} the total dissipation in the simulations with and without the monopile, respectively.

integrating the mixing rate, that is, $M = \int m dx$. The total mixing promoted by the monopile M_{OWF} is then calculated by subtracting the value of the simulations without the foundation structure M_{BBL} from the total mixing including the monopile effects M_{TOPO}, that is, $M_{OWF} = M_{TOPO} - M_{BBL}$. For all analyzed cases, the total mixing generated by one monopile is estimated to be 7–10% of the mixing induced by bottom boundary layer turbulence at the chosen domain size and is confined to the near field of the monopile. The amount of mixing that can be attributed to a foundation structure compared to the bottom boundary layer is however dependent on its geometry and on the spacing between single structures. Although the domain size chosen in this study aimed at resembling the spacing between structures currently found in the field, it is important to note that OWF with less spacing than 1,024 m between the monopiles are expected to account for more mixing relative to the bottom boundary layer. Conversely, offshore wind farms composed of more complex structures than monopiles (e.g., tripiles and tripods) are also expected to generate different mixing behavior.

3.4. Dissipation of Turbulent Kinetic Energy

We now estimate the dissipation of turbulent kinetic energy from the simulation results to better understand the mixing promoted by the OWF structures. The subgrid-scale dissipation of turbulent kinetic energy, SGS-ε, returned by the LES model gives a general impression about the level of turbulence downstream from the obstacle. However, the SGS-ε has been shown to underestimate the absolute value of the true dissipation of turbulent kinetic energy, ε, as a consequence of numerical dissipation of the advection scheme (Maronga et al., 2013). To obtain the true ε, we use the method described by Tennekes and Lumley (1973) and Maronga et al. (2013), which is based on the assumption of isotropy. The dissipation ε is thus estimated through the calculation of power spectra for a velocity component u_i on a Cartesian coordinate:

$$S_{u_i}(k) = \alpha \varepsilon^{2/3} k^{-5/3}, \tag{2}$$

with the constant $\alpha \approx 0.52$. The simulations in Maronga et al. (2013) were horizontally homogeneous, which enabled the calculation of power spectra for each depth level using all data points available at each vertical grid point. As a result, a vertical profile of ε was obtained. The monopile in our simulations is an additional source of turbulence that disrupts horizontal homogeneity, that is, the velocity fluctuations at different horizontal grid points at the same depth level cannot anymore be regarded as statistically identical. Therefore, to obtain ε, a time series of single grid points is collected instead, from which a power spectrum in the spatial domain is generated under the assumption of Taylor's hypothesis of frozen

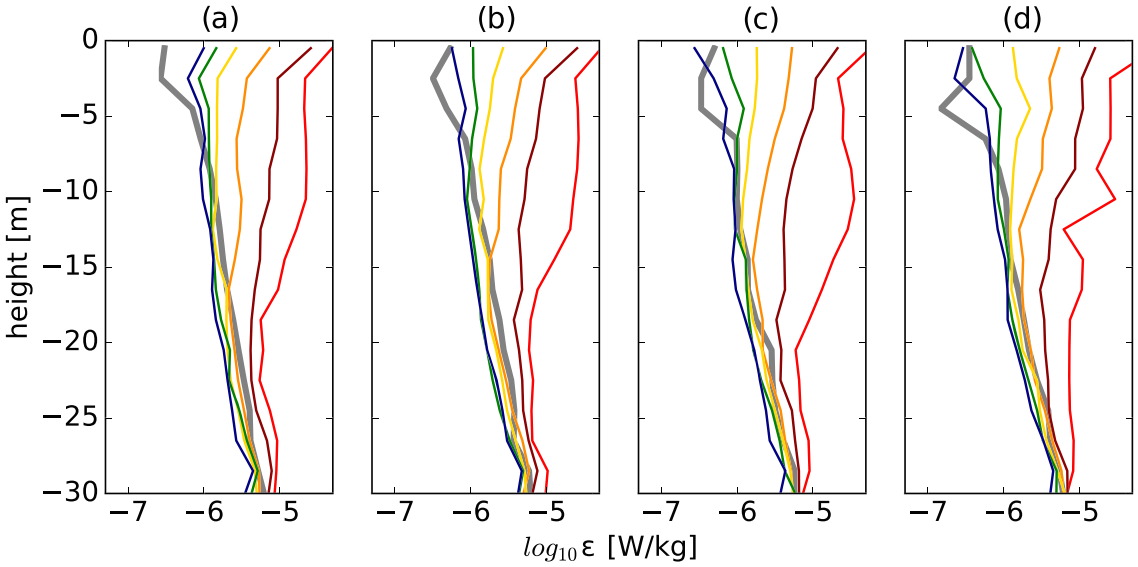

Figure 7. Vertical profiles of the dissipation of turbulent kinetic energy ε averaged within the wake of the monopile. Different colors stand for a given distance from the monopile. The colors red, dark red, dark orange, yellow, green, and blue depict profiles that are situated 60, 100, 160, 260, 360, and 460 m downstream the monopile, respectively. The thick gray lines depict ε profiles without the influence of the structure. The panels (a)–(d) refer to the four different vertical temperature gradients studied, that is, ΔT={0.5,1.5,2.5,3.5}°C, respectively.

turbulence. The usage of this method is justified by the choice of nonperiodic lateral boundary conditions (inflow and outflow) in the simulations, such that the velocity field in different grid points was statistically independent of time. Following Maronga et al. (2013), ε was calculated if an inertial subrange could be identified in the spectrum. The ε estimates obtained from the spectra compared well with the SGS-ε, although the agreement between both methods improved away from the boundaries where the eddies are not influenced by them. This was expected as the size of the large eddies decreases close to the boundaries and anisotropy becomes more prominent, thus decreasing the performance of the subgrid-scale model (Gibbs et al., 2016; Maronga et al., 2013).

Vertical profiles of ε averaged within the wake of the monopile in the different case studies are shown in Figure 7, for which the dissipation values between 725.5 and 775.5 m from the south border on the y axis were considered. The high ε ($O(10^{-6}$ W kg$^{-1})$) found in the bottom boundary layer is caused by friction at the sea bed and is comparable to that observed in field measurements at similar current magnitude (cf. Schultze et al., 2020). In all analyzed cases, ε was the highest in close proximity to the monopile, with the turbulence in the upper 10 m exceeding that of background levels by over an order of magnitude.

The total dissipation of turbulent kinetic energy attributed to the monopiles (D_{OWF}) can be estimated by subtracting the total ε of the simulations without the monopile, D_{BBL}, from those with it, D_{TOPO} (i.e., D_{OWF}=D_{TOPO}−D_{BBL}), where $D = (\rho_o/A)\int_0^{L_z}\int_0^{L_y}\varepsilon \, dy \, dz$, and A=L_yL_z is the area of each slice along the domain length. For the analyzed simulation setups, given the realistic domain size chosen, a single monopile is expected to increase the total dissipation of turbulent kinetic energy by 4–9% compared to a natural environment without the structure. Additionally, the total dissipation of each slice along the domain length demonstrates that the increase in total dissipation is concentrated within the first 200–300 m past the monopile, after which D_{TOPO} and ε itself are comparable to background levels D_{BBL} (Figures 6b and 7).

4. Discussion

4.1. Intersections Between Observations and Numerical Simulations

This study provides evidence from field measurements and numerical simulations that the wake of single offshore wind turbines is identifiable hundreds of meters downstream in terms of temperature anomalies and turbulence levels. It is, however, strongly dependent on both stratification and the quantity considered, for example, the wakes differ in size when either temperature anomaly or dissipation rate is considered.

The towed chain measurements have shown that the structure of temperature in the wake of a monopile is significantly disturbed under weak stratification (ΔT~0.5°C), which could be verified in the LES (case (i), Figure 5a). The impact of a monopile under stronger stratification is however less pronounced, which can be explained by the magnitude of the temperature anomalies generated. Moreover, while a temperature anomaly of 0.2°C is clearly visible under weak stratification of ΔT~0.5°C (i.e., $\tilde{T}/\Delta T = 0.4$), in cases with a stronger temperature gradient, for example, ΔT~1.5°C (i.e., $\tilde{T}/\Delta T = 0.13$), such a temperature anomaly could be masked by other mixing mechanisms or variability. This result helps explain the lack of a well-defined wake in the temperature field measured by the towed-chain in the stronger stratified case discussed in section 2.2. Other than very close to the monopile, the temperature anomaly caused by the structure is not strong enough to be clearly discerned from other mixing mechanisms in the field.

4.2. Bulk Mixing Efficiency

Despite the elevated turbulence levels generated by single turbines, the amount of mixing obtained is relatively low compared to BBL mixing (Figure 6). Given the total amount of mixing and turbulence attributed to a monopile, the bulk mixing efficiency can be calculated as $\eta = M_{OWF}/(M_{OWF} + \int D_{OWF} \mathrm{d}x)$. η is a bulk measure of the locally defined mixing efficiency $\gamma = R_f/(1-R_f) \approx 0.2$, where $R_f = -\mathscr{B}/\mathscr{P} = -\mathscr{B}/(-\mathscr{B} + \varepsilon)$ with $\mathscr{B}$ the buoyancy flux and $\mathscr{P}$ the shear production of turbulent kinetic energy, which is used for stratified shear flows (Gregg et al., 2018; Osborn, 1980). The mean bulk mixing efficiency η is estimated to be between 0.09–0.14 for the four studied cases and is therefore smaller than the generally accepted local value of $\gamma = 0.2$. This is explained by the fact that the turbulent mixing generated by the monopile extends through the complete vertical extent of the water column, which is not continuously stratified. Apart from the thermally stratified surface layer, the additional turbulence by the monopile then acts upon already mixed fluid, which thus decreases the overall mixing efficiency of the system. Carpenter et al. (2016) have identified the bulk mixing efficiency as a crucial parameter in the parameterization of OWF-induced mixing in larger-scale modeling efforts.

4.3. Application to the North Sea

As the tidal currents move past the OWF structures, they extract energy from the flow that is delivered to turbulence, and we define this quantity as P, in W m^{-2}. Carpenter et al. (2016) have provided estimates of the mixing potential of OWFs in the German Bight of the North Sea using this approach, and found that $P = (\rho_0 C_D A_m \langle |u^3| \rangle)/2l^2$, with l the distance between equally spaced structures, A_m the frontal area of the structure, and $\langle |u^3| \rangle$ the cubed current velocity averaged over several tidal periods. The calculations were made accounting for mean tidal current velocities and realistic OWF parameters in the German Bight, and apply per unit area within an OWF. We will carry out a rough, order of magnitude analysis here based on conditions at the North Sea Buoy 3 (NSB3), where stratification data are available. Values of P in this region were estimated to be $P_{NS} \approx 12$ mW m^{-2} and are within a factor of 2 to those at the OWF DanTysk (Carpenter et al., 2016). Note that this is based on an assumed drag coefficient of $C_D = 1.0$, which we adjust to fit with the $C_D = 0.7$ found in the present study, giving $P_{NS} = 8.4$ mW m^{-2}.

Using our estimates of the mixing efficiency by a monopile, which we take to be $\eta = 0.1$, the mixing rate of the structures can be obtained by $m_{NS} = -\eta P_{NS} \approx 0.84$ mW m^{-2}. Given P_{NS} and m_{NS} for the studied region, in the following we show how the additional mixing generated by the OWF structures could contribute to mixing a stratified water column, as well as how the additional mixing created by the structures could counteract the buildup of summer stratification.

Following Carpenter et al. (2016), a time scale can be formed for the additional OWF-induced mixing to destroy an initial stratification, quantified by φ_0, and is given by $t_{mix} = -\varphi_0/m_{NS}$. In order for this additional mixing to alter the stratification, t_{mix} must be comparable to (or less than) two other important time scales that quantify (i) the time spent within an OWF, t_{adv}, and (ii) the time required for a stratification (of magnitude φ_0) to build up, t_{build}. Estimates of these time scales have been made by Carpenter et al. (2016) and can be used with our estimates of mixing to assess a rough (order of magnitude) impact of OWFs on stratification. First, we define a representative value for the stratification to be the seasonal peak of $\varphi_0 \approx 4$ kJ m^{-2} (Carpenter et al., 2016). The time that it would take for the additional OWF-induced turbulence to mix this level of stratification away is $t_{mix} \approx 55$ days. Given that the time taken to form this level of stratification is $t_{build} \approx 60$ days, the rough equivalence of these two time scales indicates that OWF mixing could be significant

in controlling stratification. This however, relies on a stratified water column spending a significant fraction of this time within an OWF. This advective time scale, t_{adv}, is dependent on mean currents, as well as the size of OWF. Floeter et al. (2017) have estimated the residence time for drifters in a relatively small OWF of size L=8 km close to NSB3 to be t_{adv}=7–10 days. This time scale would result in a reduction of the stratification expected without an OWF by the factor t_{adv}/t_{mix}, or 13–18%. Note that as the size of OWF increases, so does this fraction. On average, we roughly expect that an OWF of size $L\approx$100 km would be needed to completely prevent the formation of stratification.

5. Considerations

The conducted simulations provided simplified case studies of OWF-induced mixing, in which sources of stabilization of the water column (e.g., heat input), and mixing mechanisms other than bottom boundary layer turbulence (e.g., wind forcing and wave breaking) have been neglected. This is justified given that our study focuses on the isolated, localized, impact of a monopile foundation structure on turbulence and mixing of a stratified water column, such that a mixing efficiency for this specific forcing field could be obtained. In addition, we have found that the turbulence and mixing generated by the structure are focused in a narrow region, with levels of turbulence that exceed that present in the surface and bottom mixed layers. This is supported by the turbulence measurements of Schultze et al. (2017), who found that *mean* levels of naturally occurring turbulent dissipation in the thermocline are of the same order of magnitude as those expected from OWFs. Since the dissipation is in fact concentrated in a narrow wake region, they are expected to dominate background conditions there. Future studies could extend the analysis by combining further destabilizing and stabilizing surface forcing mechanisms to the simulation setup and thus assess the overall rate of stratification loss in a more realistic parameter space.

By studying the impact of a single monopile, nonlinear effects of interacting wakes from different structures have been disregarded in the estimates of large-scale mixing, which should be taken as a rough estimate for the analyzed foundation type. However, considering that the increased turbulence and mixing rates attributed to the monopiles are only detected up to ~300 m past the structure, and that the stratification loss promoted by a single narrow monopile wake is small (cf. Figure 6a), the nonlinear effects of interacting wakes are expected to be small. One exception could be in conditions of weak stratification, where the wake was found to have a wider stratification anomaly (i.e., Figure 5). In this case, the downstream structures could encounter an altered stratification from the ambient. It is not clear, however, that this will result in a significant change in mixing since we have found that mixing efficiency is relatively insensitive to stratification changes. Nevertheless, nonlinear effects from wake interaction as well as other foundation types, for example, tripiles or jackets, are more complex cases and could generate different mixing conditions than single noninteracting monopiles depending on their geometry.

The scenarios analyzed in this study were composed of a bottom mixed layer that reached up until 20 m from the sea bed, where temperature stratification took over and was extended until the sea surface. This setup was chosen to enable the comparison between the field observations presented. It is known however that stratification in shelf seas is often characterized by a surface and a bottom mixed layer, which are separated by a stratified thermocline (Ross & Sharples, 2007; Schultze et al., 2017). Future studies could focus on understanding this three-layer system and how it is affected by the OWF foundations.

6. Conclusions

Offshore wind farms (OWFs) have been increasingly installed in shelf sea regions in which stratification develops. The foundation structures generate additional turbulence in the water column and are therefore an additional, anthropogenic, source of mixing. Little is known about the small-scale physical effects of such structures on the natural state, and their possible further reaching implications for primary productivity has yet to be investigated. The present study provided observational and numerical evidence of OWF-induced mixing from a small-scale perspective in a thermally stratified water column. A chain of CTDs towed by a vessel circulated around an OWF monopile to gain insight on its effect on the stratified structure of the water column. LES replicating the initial conditions found in the field experiments were conducted for comparison, with a closer analysis of the wake itself and its effect on turbulence and mixing made possible. From

the foundation structures available, the monopiles have been chosen due to their broad use and application as this type of foundation can be installed in deeper regions that become seasonally stratified.

The mixing promoted by a single monopile within a 600 m range was found to be up to 10% of that triggered by bottom boundary layer turbulence. The wake of this type of structure is characterized by a narrow region of strong turbulence within the first 50–100 m downstream, equivalent to 7–14 monopile diameters, with the dissipation of turbulent kinetic energy being 1 order of magnitude higher than the background. The elevated turbulence levels dissipate within 300 m past the monopile, after which ε becomes comparable to background levels.

The region with the sharpest decrease of background potential energy matches with the turbulence signal, and the bulk mixing efficiency lies between 9 and 14%. Knowledge of the bulk mixing efficiency allows for an order of magnitude analysis of the importance of OWFs for altering stratification in a chosen region of the North Sea. The analysis found a rough equivalence of the mixing and stratification buildup time scales, suggesting that the rate of additional mixing of the OWF structures is comparable to the rate of stratification formation in this region. However, the greatest control on this effect of OWF mixing is the relatively rapid advection of stratification through the OWFs; larger OWFs will produce greater effects on the stratification.

Future work could focus on extending the present study in various ways: (1) by complementing the present simulations with further forcing mechanisms such as wind and tidal effects; (2) assessing the impact of other foundation types and stratification conditions on turbulence and mixing; and (3) studying possible effects of enhanced scalar fluxes on primary productivity and biological activity in general.

Data Availability Statement

The temperature data is published in the FINO database (http://fino.bsh.de). Data and metadata used in this manuscript are available at http://10.0.20.161/zenodo.3874906.

Acknowledgments

This project was conducted within the Polar Regions and Coasts in the Changing Earth System II program (PACES II) funded by the Helmholtz Foundation, which we gratefully acknowledge. The authors would like to thank the support of R. Kopetzky, M. Heineke, B. Peters, T. Kock, M. Cysewski, M. Stresser, the Captain, and the crew of the research vessel (RV) *Ludwig Prandtl* and the RV *Heincke*during the towed chain measurements. The RV *Heincke* ship time was provided through the Grant AWI_HE445_00. We gratefully acknowledge the German Federal Ministry of Economic Affairs and Energy (BMWi) and the Project Management Jülich (PTJ), which provided access to the temperature measurements of the platform FINO3. We would like to thank the PALM group at the Leibniz Univertität Hannover, especially Björn Maronga and Matthias Sühring, for their support with the PALM model.

References

Arakawa, A., & Lamb, V. R. (1977). Computational design of the basic dynamical processes of the UCLA general circulation model. *Methods of Computational Physics*, *17*, 173–265.

Broström, G. (2008). On the influence of large wind farms on the upper ocean circulation. *Journal of Marine Systems*, *74*, 585–591. https://doi.org/10.1016/j.jmarsys.2008.05.001

Burchard, H., & Hofmeister, R. (2008). A dynamic equation for the potential energy anomaly for analysing mixing and stratification in estuaries and coastal seas. *Estuarine, Coastal and Shelf Science*, *77*(4), 679–687. https://doi.org/10.1016/j.ecss.2007.10.025

Carpenter, J. R., Merckelbach, L., Callies, U., Clark, S., Gaslikova, L., & Baschek, B. (2016). Potential impacts of offshore wind farms on North Sea stratification. *PLoS One*, *11*(8), e0160830. https://doi.org/10.1371/journal.pone.0160830

Cazenave, P. W., Torres, R., & Allen, J. I. (2016). Unstructured grid modelling of offshore wind farm impacts on seasonally stratified shelf seas. *Progress in Oceanography*, *145*, 25–41. https://doi.org/10.1016/j.pocean.2016.04.004

Corbetta, G., Pineda, I., & Moccia, J. (2014). The European offshore wind industry—Key trends and statistics 2013 (*Tech. Rep.*): The European Wind Energy Association. http://www.ewea.org/fileadmin/files/library/publications/statistics/European_offshore_statistics_2013.pdf

Deardorff, J. W. (1980). Stratocumulus-capped mixed layers derived from a three-dimensional model. *Boundary-Layer Meteorology*, *18*(4), 495–527. https://doi.org/10.1007/BF00119502

Floeter, J., van Beusekom, J. E. E., Auch, D., Callies, U., Carpenter, J., Dudeck, T., et al. (2017). Pelagic effects of offshore wind farm foundations in the stratified North Sea. *Progress in Oceanography*, *156*, 154–173. https://doi.org/10.1016/j.pocean.2017.07.003

Gibbs, J. A., Fedorovich, E., Maronga, B., Wainwright, C., & Dröse, M. (2016). Comparison of direct and spectral methods for evaluation of the temperature structure parameter in numerically simulated convective boundary layer flows. *Monthly Weather Review*, *144*(6), 2205–2214. https://doi.org/10.1175/MWR-D-15-0390.1

Grashorn, S., & Stanev, E. V. (2016). Kármán vortex and turbulent wake generation by wind park piles. *Ocean Dynamics*, *66*(12), 1543–1557. https://doi.org/10.1007/s10236-016-0995-2

Gregg, M. C., D'Asaro, E. A., Riley, J. J., & Kunze, E. (2018). Mixing efficiency in the ocean. *Annual review of marine science*, *10*, 443–473.

Harlow, F. H., & Welch, J. E. (1965). Numerical calculation of time-dependent viscous incompressible flow of fluid with free surface. *Physics of Fluids*, *8*, 2182–2189.

Huthnance, J. (1991). Physical oceanography of the North Sea. *Ocean and Shoreline Management*, *16*(3-4), 199–231. https://doi.org/10.1016/0951-8312(91)90005-M

Kataoka, H., & Mizuno, M. (2002). Numerical flow computation around aerolastic 3D square cylinder using inflow turbulence. *Wind Structures*, *5*, 379–392. https://doi.org/10.12989/was.2002.5.2n_3n_4.379

Ludewig, E. (2015). *On the Effect of Offshore Wind Farms on the Atmosphere and Ocean Dynamics, Hamburg Studies on Maritime Affairs 31*. Switzerland: Springer International Publishing. https://doi.org/10.1007/978-3-319-08641-5_1

Lund, T. S., Wu, X., & Squires, K. D. (1998). Generation of turbulent in-flow data for spatially-developing boundary layer simulations. *Journal of Computational Physics*, *140*, 233–258.

Maronga, B., Banzhaf, S., Burmeister, C., Esch, T., Forkel, R., Fröhlich, D., et al. (2019). Overview of the Palm Model System 6.0. *Geoscientific Model Discussion*, *13*, 1335–1372. https://doi.org/10.5194/gmd-2019-103

Maronga, B., Gryschka, M., Heinze, R., Hoffmann, F., Kanani-Sühring, F., Keck, M., et al. (2015). The parallelized large-eddy simulation model (PALM) version 4.0 for atmospheric and oceanic flows: Model formulation, recent developments, and future perspectives. *Geoscientific Model Development*, *8*(8), 2515–2551. https://doi.org/10.5194/gmd-8-2515-2015

Maronga, B., Moene, A. F., van Dinther, D., Raasch, S., Bosveld, F. C., & Gioli, B. (2013). Derivation of structure parameters of temperature and humidity in the convective boundary layer from large-eddy simulations and implications for the interpretation of scintillometer observations. *Boundary-Layer Meteorology*, *148*(1), 1–30. https://doi.org/10.1007/s10546-013-9801-6

Moeng, C.-H., & Wyngaard, J. C. (1988). Spectral analysis of large-eddy simulations of the convective boundary layer. *Journal of the Atmospheric Sciences*, *45*(23), 3573–3587. https://doi.org/10.1175/1520-0469(1988)045<3573:SAOLES>2.0.CO;2

Osborn, T. R. (1980). Estimates of the local rate of vertical diffusion from dissipation measurements. *Journal of Physical Oceanography*, *10*(1), 83–89. https://doi.org/10.1175/1520-0485(1980)010<0083:EOTLRO>2.0.CO;2

Paskyabi, M. B. (2015). Offshore wind farm wake effect on stratification and coastal upwelling. *Energy Procedia*, *80*, 131–140.

Paskyabi, M. B., & Fer, I. (2012). Upper ocean response to large wind farm effect in the presence of surface gravity waves. *Energy Procedia*, *24*, 245–254. https://doi.org/10.1016/j.egypro.2012.06.106

Raasch, S., & Schröter, M. (2001). PALM—A large-eddy simulation model performing on massively parallel computers. *Meteorologische Zeitschrift*, *10*(5), 363–372. https://doi.org/10.1127/0941-2948/2001/0010-0363

Rennau, H., Schimmels, S., & Burchard, H. (2012). On the effect of structure-induced resistance and mixing on inflows into the Baltic Sea: A numerical model study. *Coastal Engineering*, *60*(1), 53–68. https://doi.org/10.1016/j.coastaleng.2011.08.002

Ross, O. N., & Sharples, J. (2007). Phytoplankton motility and the competition for nutrients in the thermocline. *Marine Ecology Progress Series*, *347*, 21–38. https://doi.org/10.3354/meps06999

Roulund, A., Sumer, B. M., Fredsøe, J., & Michelsen, J. (2005). Numerical and experimental investigation of flow and scour around a circular pile. *Journal of Fluid Mechanics*, *534*, 351–401.

Saiki, E. M., Moeng, C.-H., & Sullivan, P. P. (2000). Large-eddy simulation of the stably stratified planetary boundary layer. *Boundary-Layer Meteorology*, *95*, 1–30.

Schultze, L. K. P., Merckelbach, L. M., & Carpenter, J. R. (2017). Turbulence and mixing in a shallow shelf sea from underwater gliders. *Journal of Geophysical Research: Ocean*, *122*, 9092–9109. https://doi.org/10.1002/2017JC012872

Schultze, L. K. P., Merckelbach, L. M., & Carpenter, J. R. (2020). Storm-induced turbulence alters shelf sea vertical fluxes. *Limnology and Oceanography Letters*, *5*(3), 264–270. https://doi.org/10.1002/lol2.10139

Simpson, J. H., & Bowers, D. (1981). Models of stratification and frontal movement in shelf seas. *Deep Sea Research Part A. Oceanographic Research Papers*, *28*(7), 727–738.

Simpson, J. H., & Sharples, J. (2012). *Introduction to the Physical and Biological Oceanography of Shelf Seas*. Cambridge: Cambridge University Press.

Tennekes, H., & Lumley, J. L. (1973). *A first course in turbulence*. Cambridge: The MIT Press.

Thomas, H., Bozec, Y., Elkalay, K., & de Baar, H. J. W. (2004). Enhanced open ocean storage of CO_2 from shelf sea pumping. *Science*, *304*(5673), 1005–1008. https://doi.org/10.1126/science.1095491

Wind Europe, B. I., Remy, T., & Mbistrova, A. (2018). The European offshore wind industry—Key trends and statistics 2017 (*Tech. Rep.*) Brussels, Belgium: Wind Europe.

Winters, K. B., Lombard, P. N., Riley, J. J., & D'Asaro, E. A. (1995). Available potential energy and mixing in density stratified fluids. *Journal of Fluid Mechanics*, *289*, 115–128. https://doi.org/10.1146/annurev-fluid-011212-140620